


Nonreciprocal Phonon Blockade in a Spinning Acoustic Ring Cavity Coupled to a Two-Level System

Xiao-Yu Yao¹, Hamad Ali, Fu-Li Li, and Peng-Bo Li^{1*}

Ministry of Education Key Laboratory for Nonequilibrium Synthesis and Modulation of Condensed Matter, Shaanxi Province Key Laboratory of Quantum Information and Quantum Optoelectronic Devices, School of Physics, Xi'an Jiaotong University, Xi'an 710049, China

 (Received 8 November 2021; revised 16 March 2022; accepted 5 April 2022; published 3 May 2022)

Quantum nonreciprocal devices have received extensive attention in recent years because they can be used to realize unidirectional quantum routing and noise isolation. In this work, we show that the shift of resonance frequencies of propagating phonons induced by spin-orbit interactions of phonons in a rotating acoustic ring cavity can be used to realize nonreciprocal phonon blockade. When driving the cavity from different directions, nonreciprocal single-, two-phonon blockade, and phonon-induced tunneling can take place by varying the parameters of the system to an appropriate value. To realize phonon blockade, a two-level system is employed to induce self-interactions of phonons in the cavity. We also show the possibility of this proposal for designing nonreciprocal phonon routing. This work provides a way to achieve acoustic nonreciprocal devices, such as directional acoustic switches and quantum noise isolation, which may help acoustic information network processing.

DOI: [10.1103/PhysRevApplied.17.054004](https://doi.org/10.1103/PhysRevApplied.17.054004)

I. INTRODUCTION

In quantum-information processing, reliable methods for creation and manipulation of phonons have become the subject of interest on account of their potential applications [1–9]. Phononic devices work in the GHz frequency range that corresponds to wavelengths on the order of μm , which makes them a bridge between optical and artificial circuits [10,11]. Thus it has the potential to be a good candidate for solid-state quantum devices [12–19]. Various methods and architectures have been investigated to study quantum phononic effects, such as phonon blockade (PB).

Phonon blockade is a phenomenon when one phonon is present in a nonlinear acoustic cavity, the subsequent phonons cannot be excited, which is one of the mechanisms to realize the single-phonon source [20]. In close analogy to Coulomb blockade [21] and photon blockade [22–27], PB is a pure quantum effect, which plays a role in unveiling the quantum behavior of a device. The initial single-phonon blockade (1PB) was achieved in a nanomechanical resonator, which is coupled to a superconducting quantum two-level system for inducing self-interactions of phonons. On this basis, great effort has been made to study other effects such as two-phonon blockade (2PB), equivalent phonon-induced tunneling (PIT), and detection of PB [28–33]. Optomechanical systems with second-order nonlinearities are considered for photon-induced phonon

blockade [28,34,35], with potential applications in hybrid photon-phonon quantum networks.

Recently, nonreciprocal devices have garnered a lot of attention [36–40]. Reciprocity is a fundamental theorem in a network, which states that when the source and observation points of the network change the positions, the response of the transmission channel is symmetric [41,42]. Nonreciprocal devices, allowing the flow of signal from one side but blocking it from the other, have become fundamental devices for building information-processing networks, such as unidirectional transmission, cloaking and noise-free information processing and amplifiers [43–52]. In classical electromagnetic networks, one usually uses magnetic materials or strong nonlinearities to destroy reciprocity [53–57]. For acoustic networks, it has been known for a long time that using moving fluids [58] or magnetic materials [59] can break reciprocity. It is reported that acoustic circulators can be realized using circulating fluids and synthetic angular momentum in acoustic meta-atoms or metamaterials [60]. And acoustic gyrators [61] and isolators [62] have been created in air pipes with steady flowing. Furthermore, acoustic nonreciprocity can also be accomplished by employing nonlinear materials [63–67]. But in quantum networks, magnetic materials are bulky and hard to integrate with other devices. And the method of using nonlinear materials is effective when driving from only one side of the system. But it is difficult to accomplish isolation when driving from both sides at the same time [68]. So in recent years, using temporal modulation to break reciprocity has received much

*lipengbo@mail.xjtu.edu.cn

attention, such as traveling-wave modulation [69–71], Sagnac effect of light [72–75], one-way Bragg mirrors [76–79], and nonreciprocal Willis coupling [80,81]. These modulations are more flexible but are still challenging experimentally to modulate precisely in time and space. Moreover, acoustic nonreciprocity has also been suggested as a result of topologically protected edge states [76,82–88], elastic solitons [89], and acoustic radiation pressure [90]. But so far, the nonreciprocal phonon blockade has yet to be realized.

In this work, we study nonreciprocal PB and PIT in nonstationary ring resonators, having counterpropagating traveling acoustic modes coupled to a two-level system (TLS). The TLS-phononic system, which can be regarded as a phonon cavity QED system, may provide a promising setup for realizing nonreciprocal PB. To be specific, we use a two-level system to induce phonon self-interactions in the rotating ring cavity. We find that, nonreciprocal 1PB and PIT can be induced in the spinning ring resonator when driving it from the left or right side of a coupled phononic waveguide, because the cavity phonons satisfy the sub-Poisson distribution or the super-Poisson distribution. Furthermore, by varying other parameters of the system, we can get other nonreciprocal phenomena such as 2PB and multi-PB. The physical origins behind the nonreciprocity phenomena are the spin-orbit interaction (SOI) of phonons in the spinning ring resonator. It causes a shift in the resonance frequency and phase of the propagating phonon mode in the cavity, which has been proved in recent experiments [91]. Compared to other nonreciprocal schemes, the proposed setup can easily tune the nonreciprocity just by adjusting the angular frequency and other experimental parameters. Such nonreciprocal PB can be used for many acoustic devices, such as acoustic diodes [92–96], which can play a key role in a phonon-basis information network at the few-phonon levels [97].

The remainder of this paper is organized as follows. In Sec. II, we describe the physical model of an acoustic ring resonator coupled to a two-level system. In Sec. III, we present phonon blockade in the case of the stationary ring resonator coupled to the two-level system. In Sec. IV, we present our result in the case of the rotating system. In Sec. V, we show the possibility of designing nonreciprocal routing through our proposal. Experimental feasibility of our scheme is given in Sec. VI. Finally, the conclusion is given in Sec. VII.

II. MODEL

The system we consider consists of an acoustic ring cavity coupled to a phononic waveguide and to a TLS at the same time, as illustrated in Fig. 1. Under the rotating-wave approximation and neglecting two-phonon terms, the Hamiltonian of such a system is given by

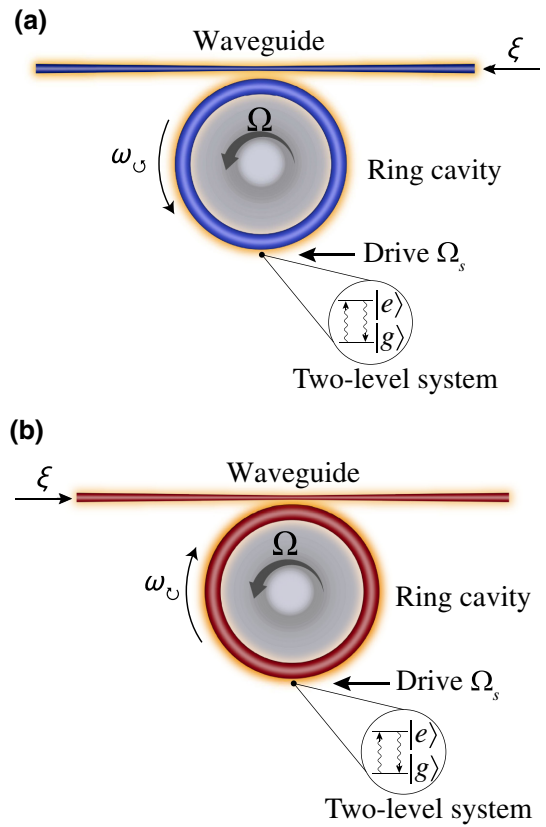


FIG. 1. Schematic of the composite spin-phononic system. The ring cavity is coupled with the phononic waveguide to the input and output of the driving field, and at the same time coupled to a two-level system to realize phonon blockade. In addition, we add a rotator to the cavity to make the cavity rotate counterclockwise at an angular frequency Ω . The phonons, which input from the left or right side of the waveguide, rotate counterclockwise or clockwise in the cavity corresponding to (a) or (b), respectively.

$$\begin{aligned}
 H^{(0)} &= \hbar\omega a^\dagger a + \frac{1}{2}\hbar\omega_0\sigma_z + \hbar g (a\sigma_+ + a^\dagger\sigma_-) \\
 &\quad + \hbar\Omega_s (\sigma_+ e^{-i\omega_1 t} + \sigma_- e^{i\omega_1 t}), \\
 H^{(d)} &= \hbar\xi (a^\dagger e^{-i\omega_L t} + a e^{i\omega_L t}).
 \end{aligned} \tag{1}$$

Here, ω is the resonance frequency of the cavity, $a(a^\dagger)$ denote the annihilation (creation) operator of the cavity field, $\hbar\omega_0$ is the level splitting of the two-level system, which is described by the spin operator $\sigma_z = |e\rangle\langle e| - |g\rangle\langle g|$, with $|e\rangle$ and $|g\rangle$ representing the excited and ground state of the TLS, respectively. The ladder operators $\sigma^\pm = 1/2(\sigma^x \pm i\sigma^y)$ describe the interaction between the TLS and the phononic cavity, with σ^x and σ^y as Pauli matrices, where g is the coupling strength between the cavity mode and the TLS. The parameter ξ is the driving-field amplitude with driving frequency ω_L .

We consider the regime where the TLS and phonon modes are far detuned to the coupling strength $\Delta =$

$(\omega - \omega_0) \gg g$ and the Rabi frequency Ω_s , by which the TLS is driven with the field of frequency ω_1 , obeys the condition $\Omega_s \gg (g^2/\Delta)$. Here we assume that $\omega_1 = \omega_0$, and then the Hamiltonian $H^{(0)}$ in Eq. (1) in the rotating frame with $V = \exp(-i\omega_0\sigma_z t/2)$ can be written as [20,98]

$$H_{\text{eff}}^{(0)} = \hbar\omega a^\dagger a + \hbar U a^\dagger a^\dagger a a, \quad (2)$$

with the effective phonon-phonon interaction term (nonlinearity strength)

$$U = \frac{g^4}{\Omega_s \Delta^2}. \quad (3)$$

Here, it is worth mentioning that after straightforward calculations we ignore $\rho_z = |+\rangle\langle+| - |-\rangle\langle-|$, with $|\pm\rangle = (|g\rangle \pm |e\rangle)/\sqrt{2}$, by preparing the TLSs in the ground state $|-\rangle$.

In the ring cavity, the phonon modes with two different propagation directions [clockwise (CW) or counterclockwise (CCW), corresponding to driving of the cavity from the left- or right-hand side, respectively] carry different orbital angular momentum (OAM) [91,99]. The phonon in different propagation directions will possess spins of opposite direction because of SOI. Therefore, phonons propagating CW or CCW experience the centripetal or centrifugal Coriolis force, respectively [100]. When we add a rotator that rotates CCW at the angular frequency Ω to the cavity, the resonant frequency of phonons will have a change, i.e., $\omega \rightarrow \omega + \Delta_F$, where

$$\Delta_F = \chi\Omega, \quad (4)$$

where $\chi = \pm 0.12$ is the chirality of the phonon. For the rotator, rotating in the CCW direction, when the cavity phonon rotates CW, $\Delta_F > 0$, otherwise, $\Delta_F < 0$. Now in the rotating reference frame at the driving frequency ω_L , the effective Hamiltonian of the driven system can be written as

$$H_{\text{eff}} = \hbar(-\Delta_L + \Delta_F) a^\dagger a + \hbar U a^\dagger a^\dagger a a + \hbar\xi (a^\dagger + a), \quad (5)$$

where $\Delta_L = \omega_L - \omega$ is the detuning between the field of the nonrotation resonant cavity and the driving field.

In order to obtain the analytical solution of the system, we first consider the isolated phononic system. We have

$$H_{\text{eff}} = \hbar(-\Delta_L + \Delta_F) a^\dagger a + \hbar U a^\dagger a^\dagger a a. \quad (6)$$

For a Fock state $|n\rangle$, we have

$$\begin{aligned} H_{\text{eff}}|n\rangle &= [-\hbar\Delta_L \hat{a}^\dagger \hat{a} + \hbar\Delta_F \hat{a}^\dagger \hat{a} + \hbar U a^\dagger a^\dagger a a] |n\rangle \\ &= [-\hbar\Delta_L \hat{a}^\dagger \hat{a} + \hbar(\Delta_F - U) \hat{a}^\dagger \hat{a} + \hbar U \hat{a}^\dagger \hat{a} \hat{a}^\dagger \hat{a}] |n\rangle \\ &= [-n\hbar\Delta_L + n\hbar(\Delta_F - U) + n^2\hbar U] |n\rangle \\ &= E_n |n\rangle. \end{aligned}$$

Thus we obtain the eigenenergy

$$E_n = -n\hbar\Delta_L + n\hbar\Delta_F + (n^2 - n)\hbar U, \quad (7)$$

where n is the number of cavity phonons. The eigenenergy is also effective for the weak-driving condition. In the region of weak drive $\xi \ll \gamma$, we can truncate the Hilbert space of the system to $n = 2$. Here, $\gamma = \omega/Q$ is the cavity dissipation rate and Q is the quality factor. The state of the system can be written as $|\varphi(t)\rangle = \sum_{n=0}^2 C_n(t)|n\rangle$, where C_n is the probability amplitude. For the effective Hamiltonian, Eq. (5), we can introduce a dissipation term according to the quantum-trajectory method [101]: $H = H_{\text{eff}} - (i\hbar\gamma/2)\hat{a}^\dagger \hat{a}$. Then the equation of motion of the dissipative system is given by

$$\begin{aligned} \dot{C}_0(t) &= -i\frac{E_0}{\hbar}C_0(t) - i\xi C_1(t), \\ \dot{C}_1(t) &= -i\left(\frac{E_1}{\hbar} - i\frac{\gamma}{2}\right)C_1(t) - i\xi C_0(t) - i\xi\sqrt{2}C_2(t), \\ \dot{C}_2(t) &= -i\left(\frac{E_2}{\hbar} - i\gamma\right)C_2(t) - i\xi\sqrt{2}C_1(t). \end{aligned} \quad (8)$$

With the initial conditions: $C_0(0) = 1$ and $C_1(0) = C_2(0) = 0$, the steady-state solutions of the system can be derived as

$$\begin{aligned} C_1(\infty) &= \frac{-\xi}{\left(\frac{E_1}{\hbar} - \frac{E_0}{\hbar} - i\frac{\gamma}{2}\right)}, \\ C_2(\infty) &= \frac{-\sqrt{2}\xi C_1(\infty)}{\left(\frac{E_2}{\hbar} - \frac{E_0}{\hbar} - i\gamma\right)}. \end{aligned} \quad (9)$$

Now we proceed to study PB and PIT. For this purpose, we exploit the μ^{th} -order correlation function of zero-time delay $g^{(\mu)}(0) \equiv \langle \hat{a}^{\dagger\mu} \hat{a}^\mu \rangle / \langle \hat{n} \rangle^\mu$, with $\hat{n} = \hat{a}^\dagger \hat{a}$. Describing the probability of finding n phonons in the acoustic cavity by $P(n) = |C(n)|^2$, we can define the correlation function as follows:

$$\begin{aligned} g^{(2)}(0) &= \frac{2P_2}{(P_1 + 2P_2)^2} \\ &\simeq \frac{(-\Delta_L + \Delta_F)^2 + \gamma^2/4}{(-\Delta_L + \Delta_F + U)^2 + \gamma^2/4}. \end{aligned} \quad (10)$$

For $n = 3$, we can get the third-order correlation function

$$g^{(3)}(0) = \frac{6P_3}{(P_1 + 2P_2 + 3P_3)^3} \simeq \frac{\left[(-\Delta_L + \Delta_F)^2 + \frac{\gamma^2}{4}\right]^2}{\left[(-\Delta_L + \Delta_F + U)^2 + \frac{\gamma^2}{4}\right] \left[(-\Delta_L + \Delta_F + 2U)^2 + \frac{\gamma^2}{4}\right]}. \quad (11)$$

The minimum and the maximum of $g^{(\mu)}(0)$ are corresponding to 1PB, multi-PB, and PIT, respectively. For example, when $g_{\min}^{(2)}(0) = 1/[4(U/\gamma)^2 + 1] < 1$ for $\Delta_L = \Delta_F$, the phonons satisfy the super-Poisson distribution (phonon bunching state), which corresponds to 1PB; when $g_{\max}^{(2)}(0) = 4(U/\gamma)^2 + 1 > 1$ for $\Delta_L = \Delta_F + U$, the phonons satisfy the sub-Poisson distribution (phonon antibunching state), which corresponds to PIT. For $\mu > 2$, we have similar results for multi-PB and PIT.

III. PHONON BLOCKADE

In this section, we study the realization of PB in the hybrid quantum system including the dissipation effect. The master equation for the system is given as

$$\dot{\hat{\rho}} = \frac{i}{\hbar}[\hat{\rho}, H_{\text{eff}}] + \frac{\gamma}{2}(2\hat{a}\hat{\rho}\hat{a}^\dagger - \hat{a}^\dagger\hat{a}\hat{\rho} - \hat{\rho}\hat{a}^\dagger\hat{a}), \quad (12)$$

where H_{eff} is the Hamiltonian given in Eq. (5). We can get the phonon-number probability $P(n) = \langle n | \hat{\rho} | n \rangle$ from the steady-state solution $\hat{\rho}$ of the system.

We now focus on the properties of the cavity phonons described by the second-order correlation function for various driving-field strengths ξ . In Fig. 2 we plot the results given by Eq. (12) as a function of the nonlinear strength U and detuning Δ_L in the case of a stationary cavity, i.e., $\Delta_F = 0$. In the weak-drive condition ($\xi = 0.33\gamma$), one can easily see the maximum and minimum regions of the second-order correlation function shown in Fig. 2(a). The multiple relative maximum curves in Figs. 2(b)–2(d) corresponding to $\xi = 1\gamma$, $\xi = 3\gamma$, and $\xi = 5\gamma$, respectively, are derived from the contribution of multiphonon resonances rather than just two-phonon resonance; this effect does not appear in the weak-drive case. At this time, the entire system is equivalent to a conventional PB model. Here we introduce a standard criterion for judging PB and PIT [102–104].

For n -phonon blockade (n PB), there is

$$\begin{aligned} (i) \quad & g^{(n+1)}(0) < \exp(-\langle \hat{m} \rangle) = f, \\ (ii) \quad & g^{(n)}(0) \geq \exp(-\langle \hat{m} \rangle) + \langle \hat{m} \rangle \cdot g^{(n+1)}(0) = f^{(n)}, \end{aligned} \quad (13)$$

for PIT, there is

$$g^{(\mu)}(0) > \exp(-\langle \hat{m} \rangle), \quad \text{for } \mu \geq 2. \quad (14)$$

Here, $\langle \hat{m} \rangle$ is the average phonon number of the cavity field.

In this work, we mainly consider the situation where the number of phonons is small ($n \leq 4$). In this case, $\langle \hat{m} \rangle \ll 1$, so Eq. (14) can be rewritten as

$$g^{(\mu)}(0) > 1, \quad \text{for } 4 \geq \mu \geq 2. \quad (15)$$

For n PB, we also have an equivalent standard for comparing the phonon-number distribution with the Poisson distribution:

$$\begin{aligned} (i) \quad & P(m) < \mathcal{P}(m), \quad \text{for } m > n, \\ (ii) \quad & P(n) \geq \mathcal{P}(n), \end{aligned} \quad (16)$$

with $\mathcal{P}(n) = \frac{\langle \hat{m} \rangle^n}{n!} \exp(-\langle \hat{m} \rangle)$ is the Poissonian distribution. To show a relative deviation of a given phonon-number distribution from the corresponding Poissonian distribution, we use the formula [104]

$$[P(n) - \mathcal{P}(n)]/\mathcal{P}(n). \quad (17)$$

To further elaborate the effect of weak drive on PB in the nonrotating system ($\Delta_F = 0$), in Fig. 3 we plot the n -order correlation function for constant nonlinear strength (U). Figure 3(a) shows the results for the n -order correlation function with respect to the detuning (Δ_L) for $U = 20\gamma$.

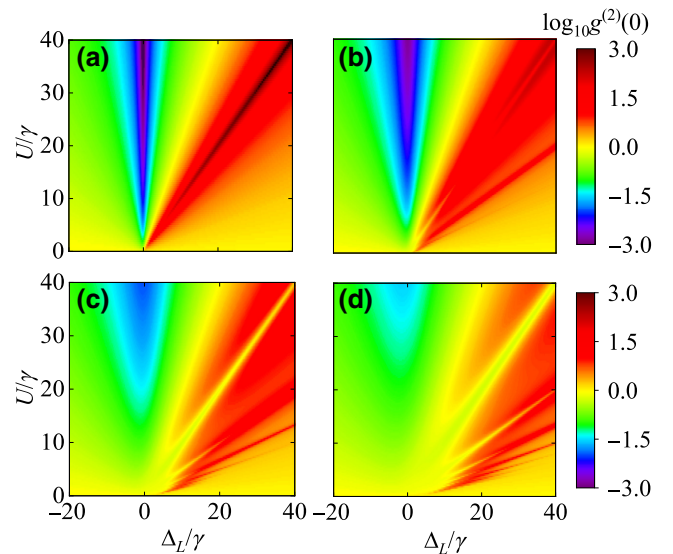


FIG. 2. $g^{(2)}(0)$ as a function of the nonlinear strength U and the detuning Δ_L , here $\Delta_F = 0$. (a),(b),(c),(d) corresponds to the situation when $\xi = 0.33\gamma$, $\xi = 1\gamma$, $\xi = 3\gamma$, and $\xi = 5\gamma$, respectively.

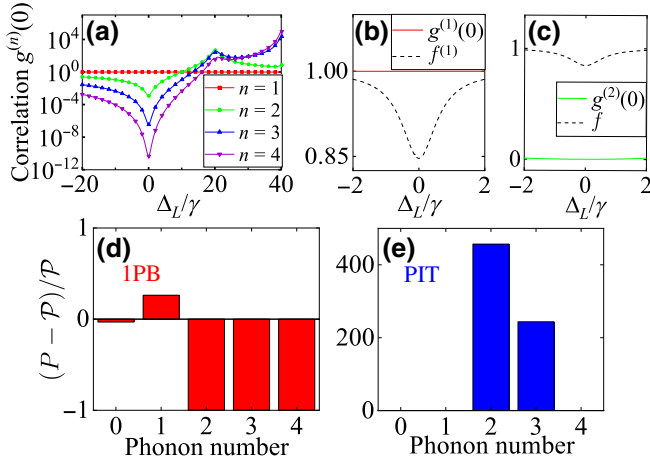


FIG. 3. (a) Under the weak-driving-strength region $\xi = 0.33\gamma$, the correlation function versus the detuning Δ_L at $U = 20\gamma$. (b),(c) show the comparison for 1PB between the correlation function and the standard value in Eq. (18). (d),(e) show the deviation between the phonon population and the Poisson distribution for 1PB and PIT, respectively at $\Delta_L = 0$ and $\Delta_L = 20\gamma$.

Here, for $g^{(2)}(0)$, the minimum and maximum values are at $\Delta_L = 0$ and $\Delta_L = 20\gamma$, which corresponds to 1PB and PIT, respectively.

According to Eq. (13), 1PB should meet the following conditions for $n = 1$:

$$\begin{aligned} (i) \quad & g^{(2)}(0) < \exp(-\langle \hat{m} \rangle) = f, \\ (ii) \quad & g^{(1)}(0) \geq \exp(-\langle \hat{m} \rangle) + \langle \hat{m} \rangle \cdot g^{(2)}(0) = f^{(1)}. \end{aligned} \quad (18)$$

Next, in Figs. 3(b) and 3(c) we plot the n -order correlation functions and standard values given in Eq. (18) as functions of Δ_L . We find that the curves of the correlation function satisfy the conditions in Eq. (18). Furthermore, in Fig. 3(d), we find that $P(1) > \mathcal{P}(1)$, $P(2) < \mathcal{P}(2)$, and $P(3) < \mathcal{P}(3)$, which is a clear signature of 1PB. Due to PIT corresponding to the super-Poisson distribution of phonons, we can find that $P(2) > \mathcal{P}(2)$ and $P(3) > \mathcal{P}(3)$ in Fig. 3(e). In addition, we can find that $g^{(2)}(0) > g^{(3)}(0) > g^{(4)}(0) > 1$ in Fig. 3(a), which indicates the emergence of PIT at this time.

Now we investigate PB under strong drive conditions depicted in Fig. 4. Figure 4(a), shows the results for the n -order correlation function versus the detuning (Δ_L) for $U = 20\gamma$ and $\xi = 3\gamma$. One can see the system still shows 1PB at $\Delta_L = 0$. Unlike the aforementioned case in Fig. 3(a), one may notice that there is second minimum in the correlation curves in Fig. 4(a), corresponding to two-phonon blockade. The results of 2PB and PIT can be seen at $\Delta_L = 20\gamma$ and $\Delta_L = 40\gamma$, respectively.

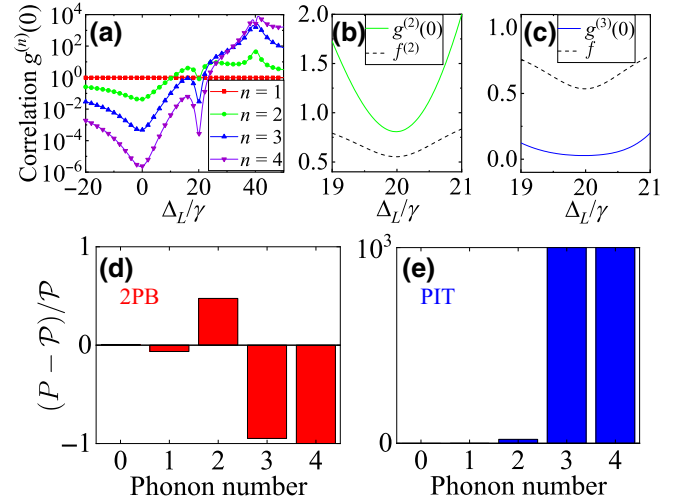


FIG. 4. (a) Under the strong-driving region $\xi = 3\gamma$, the correlation function versus the detuning Δ_L at $U = 20\gamma$. (b),(c) show the comparison for 2PB between the correlation function and the standard value in Eq. (19). (d),(e) show the deviation between the phonon population and the Poisson distribution for 2PB and PIT, respectively at $\Delta_L = 20\gamma$ and $\Delta_L = 40\gamma$.

According to Eq. (13), 2PB should meet the following conditions for $n = 2$:

$$\begin{aligned} (i) \quad & g^{(3)}(0) < \exp(-\langle \hat{m} \rangle) = f, \\ (ii) \quad & g^{(2)}(0) \geq \exp(-\langle \hat{m} \rangle) + \langle \hat{m} \rangle \cdot g^{(3)}(0) = f^{(2)}. \end{aligned} \quad (19)$$

In Figs. 4(b) and 4(c) we show the correlation function versus the detuning Δ_L , which satisfies the conditions in Eq. (19). Further, in Fig. 4(d), we can see $P(2) > \mathcal{P}(2)$, $P(3) < \mathcal{P}(3)$, and $P(4) < \mathcal{P}(4)$, which meets our criterion given in Eq. (16) for $n = 2$. Here, we can see that $P(3) > \mathcal{P}(3)$ and $P(4) > \mathcal{P}(4)$ in Fig. 4(e). Different from Fig. 3(a), here $g^{(4)}(0) > g^{(3)}(0) > g^{(2)}(0) > 1$ in Fig. 4(a), corresponding to three-phonon resonance, because of the significant increase in the drive strength. It is worth mentioning that the PIT at $\xi = 0.33\gamma$ [Fig. 3(a)] corresponds to the 2PB at $\xi = 3\gamma$, which can explain the emergence of the hollow window of the maximum area in Figs. 2(b) and 2(c), i.e., the transformation of PIT to PB by enhancing the driving strength. This can illustrate the equivalence of PB and PIT.

IV. NONRECIPROCAL EFFECT

Now, let us consider the effect of rotating the cavity. In Fig. 5 we plot the correlation function $g^{(2)}(0)$ as a function of the detuning Δ_L when the angular velocity Ω takes various values in the weak-driving regime. In Fig. 5(a) [Fig. 5(b)] we can see the correlation curves shift to the left (right) after the angular velocity Ω increases. Thus, the rotation of the cavity is the source of reciprocity, which

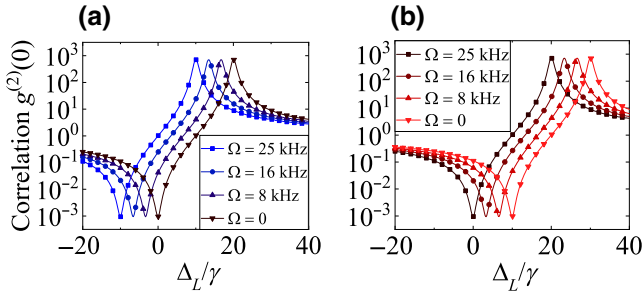


FIG. 5. The correlation function $g^{(2)}(0)$ versus the detuning Δ_L under weak driving $\xi = 0.33\gamma$ and nonlinear constant $U = 20\gamma$. (a) and (b) is corresponding to the results of driving the cavity from the right side and the left side of the waveguide, respectively.

causes the input driving from two different directions to have different resonance frequencies in the cavity.

By choosing the appropriate rotational angular velocity Ω , we can make different quantum effects appear at the same time. As shown in Fig. 6(a), we have 1PB that appears when driving from one side, and PIT, which indicates that the absorption of the first phonon enhances the absorption of subsequent phonons and appears when driving from the other side at $\Delta_F = \Delta_L = U/2 = 10\gamma$. Furthermore, Fig. 6(a) shows that our analytical solution and the numerical solution are consistent; here we use $g_{\circlearrowleft}^{(2)}(0)$ and $g_{\circlearrowright}^{(2)}(0)$ to indicate that $\Delta_F > 0$ and $\Delta_F < 0$, respectively. We can clearly see that at $\Delta_L = 10\gamma$, there is 1PB when driving the system from the left side, and PIT when driving the system from the right side, which is conformance to our expectation. For the difference of $g^{(2)}(0)$ for opposite directions, there is nonreciprocity with up to 6 orders of magnitude. This magnitude depends on the intensity of nonlinearity, which can be proved in Fig. 2. In Fig. 6(b), we can intuitively understand the reason why we have 1PB and PIT by considering the change of energy-level structure of the system.

In Fig. 7, we show the correlation function versus the detuning Δ_L in the strong-driving regime ($\xi = 3\gamma$) for $\Delta_F = 10\gamma$. The solid curves represent the result of $g_{\circlearrowleft}^{(n)}(0)$, and the dashed line represents the result of $g_{\circlearrowright}^{(n)}(0)$. Here, at $\Delta_L = 10\gamma$, we have 1PB and 2PB for the different driving directions. Furthermore, at $\Delta_L = 30\gamma$, we obtain 2PB and PIT caused by the three-phonon resonance for different driving directions. These results are discussed in detail in Figs. 8 and 9.

In Fig. 8(a), we can intuitively understand the reason why we have 1PB and 2PB by considering the energy-level structure of the system. The plots in Figs. 8(b) and 8(c) show the comparison of correlation functions [$g^2(0)$ and $g^3(0)$] with the standard values given in Eq. (19) for strong-driving strengths. We find that the curves of correlation functions satisfy the 2PB equation given in Eq.

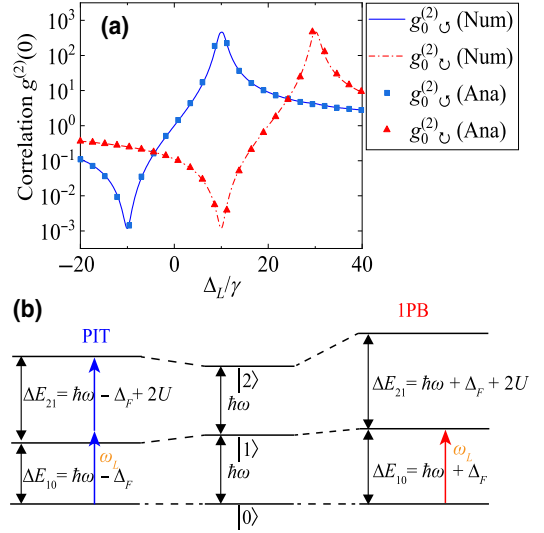


FIG. 6. (a) The correlation function $g^{(2)}(0)$ versus the detuning Δ_L with $\xi = 0.33\gamma$, $\Delta_F = 10\gamma$, and $U = 20\gamma$. The chain (solid) line is the numerical solution result of driving the system from the left (right) side, and the triangle (square) scatter is the analytical solution result of driving the system from the left (right) side. (b) The energy levels of driving the system from the left side and driving the system from the right side become nonequidistant at $\Delta_L = 10\gamma$.

(19). Moreover, in Fig. 8(d), we can find that $P(2) > \mathcal{P}(2)$, $P(3) < \mathcal{P}(3)$, and $P(4) < \mathcal{P}(4)$, which meets the criterion given in Eq. (16) for $n = 2$. In Fig. 8(e), we find that $P(1) > \mathcal{P}(1)$, $P(2) < \mathcal{P}(2)$, and $P(3) < \mathcal{P}(3)$, which meets the criterion in Eq. (16) for $n = 1$.

Next in Fig. 9(a), we show the energy-level structure of the system, which enables us to understand the nonreciprocity of 2PB and PIT. Similarly in Figs. 9(b) and 9(c), we show that the curves of the correlation function satisfy the results given in Eq. (19). Furthermore, we can

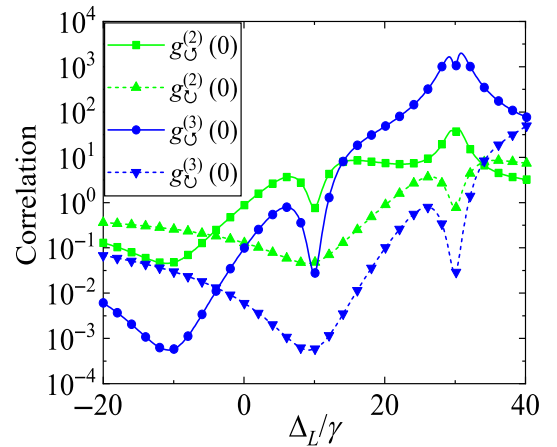


FIG. 7. The correlation function versus the detuning Δ_L with $\xi = 3\gamma$, $\Delta_F = 10\gamma$, and $U = 20\gamma$.

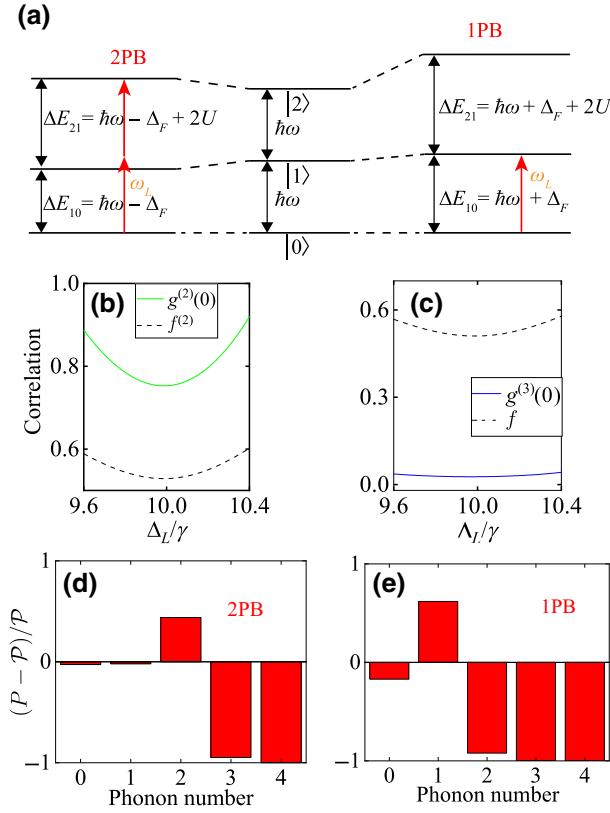


FIG. 8. (a) Energy levels of driving the system from the left and driving the system from the right side become nonequidistant for $\Delta_L = 10\gamma$. (b),(c) show the comparison for 2PB between the correlation function and the standard value in Eq. (19), (d),(e) show the deviation of the phonon population and the Poisson distribution for 1PB and 2PB, respectively.

see that $P(3) > \mathcal{P}(3)$ and $P(4) > \mathcal{P}(4)$ in Fig. 9(d). In Fig. 9(e), one can clearly see that $P(2) > \mathcal{P}(2)$, $P(3) < \mathcal{P}(3)$, and $P(4) < \mathcal{P}(4)$, which meets the criterion given in Eq. (16) for $n = 2$. In addition to the above results, we can also obtain nonreciprocity of 1PB and PIT caused by three-phonon resonance at $\Delta_F = 20\gamma$ and $\Delta_L = 20\gamma$, nonreciprocity of 2PB and PIT caused by four-phonon resonance at $\Delta_F = 20\gamma$ and $\Delta_L = 40\gamma$ for $U = 20\gamma$.

V. APPLICATION: PHONON ROUTERS

In this section, we show how to utilize our scheme to design a nonreciprocal phonon router. We first consider the most common case, as shown in Fig. 10(a), where the resonator is directly coupled to the waveguide without adding any effect. In this case, phonons input from either end of the waveguide can pass through the waveguide and output from the other end. This is the simplest transport network. Then, we consider the case after adding the drive to the two-level system. In Fig. 10(b), we show the results of the system under the nonlinearity of 1PB, and the specific parameters are the same as those of the system at the

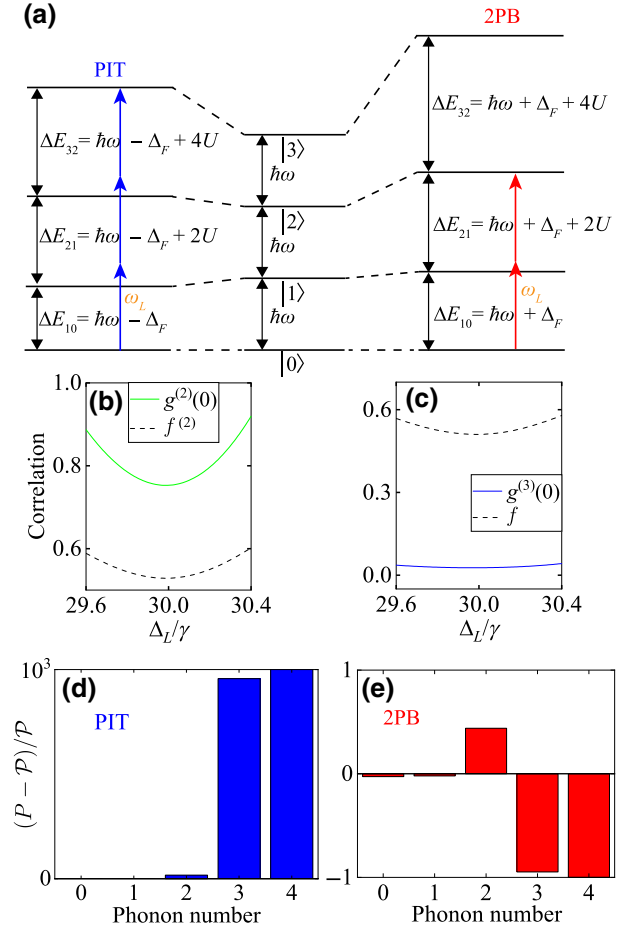


FIG. 9. (a) Under the strong-driving-strength region $\xi = 3\gamma$, the energy levels of driving the system from the left and driving the system from the right side become nonequidistant for $\Delta_L = 30\gamma$. (b),(c) show the comparison for 2PB between the correlation function and the standard value in Eq. (19), (d),(e) show the deviation of the phonon population and the Poisson distribution for 2PB and PIT, respectively.

1PB case in Fig. 3. In this case, our system can be used to implement single-phonon routing, with the system only allowing input phonons to travel in the waveguide as single phonons. The system in this situation can also be used to realize two-phonon routing by adjusting the parameters to realize the 2PB effect as shown in Fig. 4.

Next, we discuss the impact of nonreciprocity on the router. As shown in Fig. 10(c), the system has a nonreciprocity of 1PB and PIT, and the parameters are the same as those in Fig. 6. When phonons are input from the left side of the system, they can only be output as a single phonon from the right end. When phonons are input from the right, they can be output in the form of two or more phonons from the left. We achieve nonreciprocal single-phonon routing at this stage. When we adjust the system to the case shown in Fig. 8, that is, with a nonreciprocity of 1PB and 2PB, the system becomes a nonreciprocal

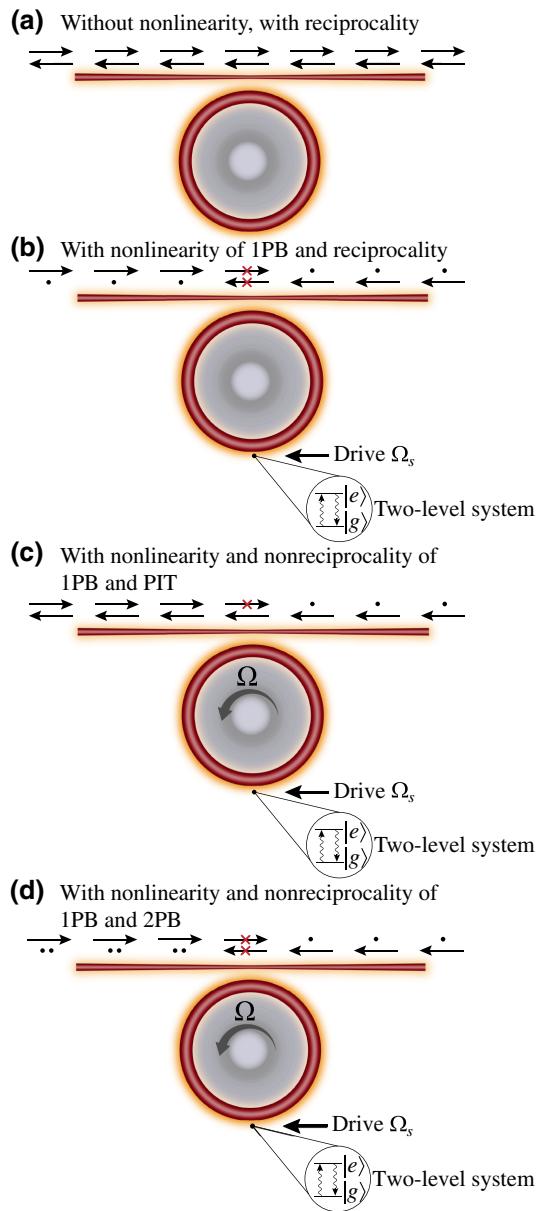


FIG. 10. (a) Phonons input from both sides of the waveguide can be transmitted to the other end. (b) The phonons input from both sides of the waveguide can only be transmitted to the other end in the form of a single phonon. (c) Phonons input from both sides of the waveguide, one side can be transmitted to the other end, and the other side can only be transmitted to the other end in the form of a single phonon. (d) For phonons input from both sides of the waveguide, one side can only be transmitted to the other end in the form of a single phonon, and the other side can only be transmitted to the other end in the form of two phonons.

few-phonon routing, with a single-phonon output when inputting phonons from the left and at most two phonons output when inputting phonons from the right, as shown in Fig. 10(d). The distinction between these two systems under nonreciprocity is that the former allows output in

the form of three phonon, whilst the latter does not. Similarly, by modifying the system parameters to different states, we can achieve few-phonon routing with different nonreciprocity.

VI. EXPERIMENTAL FEASIBILITY

For examining the feasibility of this scheme in the experiment, we now discuss the relevant parameters. In Fig. 11, we offer an example of a possible experimental setup schematic. The phononic waveguides and annular cavities, made of piezoelectric materials, are fabricated on a substrate, and they are coupled by a wrap-around coupler. Interdigital transducers at both ends of the waveguide can input and output phonons. Two-level qubits can be fabricated inside or on the surface of the substrate to couple with the ring cavity. Commonly used piezoelectric materials are ZnO, AlN, and GaN [105,106], and optional substrate materials are silicon, sapphire, diamond, and other wide-band-gap semiconductors [107–109].

Manufacturing technology for surface-acoustic-wave devices has advanced, and the manufacture of waveguides and ring cavities is no longer difficult [110,111]. In our calculations, the resonance frequency of the cavity is $\omega/2\pi = 2.25$ GHz, and the quality factor is $Q = 1.5 \times 10^7$ [112]. The rotation of the device can be solved by mounting the device on a rotating stage, which has been achieved in recent experiments [91].

Phonons in the surface-acoustic-wave devices can couple to various qubits, such as quantum dots, N-V, and Si-V centers in diamond [113–125]. Quantum dot is a suitable choice for our strategy, as it can be well characterized by an efficient two-level system [126]. It is strongly coupled to phonons, with a coupling strength of 100 MHz [127]. Another intriguing system that matches our approach is N-V and Si-V centers in diamond [128–131]. Experiments have demonstrated the fabrication of GaN

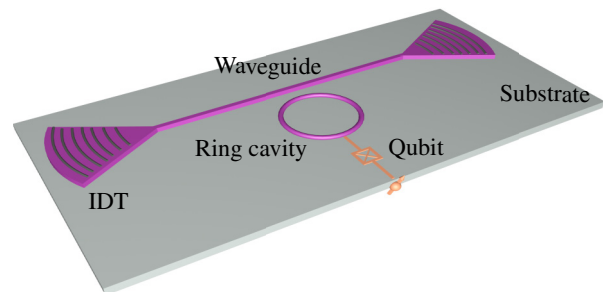


FIG. 11. Possible setup for experimental implementation. Surface acoustic waves can be generated by an interdigital transducer (IDT), which travel via a waveguide and output from the IDT at the other end. Epitaxially grown layers of piezoelectric material make up the waveguide and ring cavity. Qubits fabricated on or inside the substrates, such as superconducting qubits, or spin qubits, can be used to realize the qubit-phonon coupling.

(ZnO/AlN)/diamond heterostructures and implantation of N-*V*/Si-*V* centers in the shallow (10 nm below the surface) of diamond [132–136]. The coupling strength is usually in the MHz range [137]. Superconducting qubits are ideal for regulating and measuring quantum states in mechanical resonators due to their microwave transition frequencies, and the coupling strength is also in the MHz range [138–141]. According to Eq. (3), the coupling strength on the order of MHz can induce nonlinearity on the order of 10 kHz, which is enough to achieve phonon blockade.

VII. CONCLUSION

In conclusion, we study the nonreciprocal phonon blockade in a spinning acoustic ring resonator coupled to a two-level system. We show that in this hybrid system, the SOI of phonons causes a nonreciprocal response. The statistical properties of phonons are exploited through calculating the higher-order correlation functions. We investigate the PB for various system parameters like the nonlinearity strength, driving strength, and drive frequency in a cavity rotating in the CCW direction. We find that in the weak-driving regime, nonreciprocity of 1PB and PIT for CW and CCW modes occurs, respectively. For strong driving we obtain nonreciprocity of 1PB and 2PB with the same system parameters. Furthermore, in the strong-driving regime we have nonreciprocity of 2PB and PIT for CW and CCW modes, respectively. We also show the possibility of achieving nonreciprocal few-phonon routing by our scheme. These results combined with the current quantum technologies can be used to implement nonreciprocal few-phonon sources, nonreciprocal phonon routers, and other quantum unidirectional devices.

ACKNOWLEDGMENTS

This work is supported by the National Natural Science Foundation of China under Grant No. 92065105 and Natural Science Basic Research Program of Shaanxi (Program No. 2020JC-02).

-
- [1] T. A. Palomaki, J. D. Teufel, R. W. Simmonds, and K. W. Lehnert, Entangling mechanical motion with microwave fields, *Science* **342**, 710 (2013).
- [2] H. Okamoto, A. Gourgout, C. Y. Chang, K. Onomitsu, I. Mahboob, E. Y. Chang, and H. Yamaguchi, Coherent phonon manipulation in coupled mechanical resonators, *Nat. Phys.* **9**, 480 (2013).
- [3] H. Jing, S. K. Ozdemir, X. Y. Lu, J. Zhang, L. Yang, and F. Nori, Pt-Symmetric Phonon Laser, *Phys. Rev. Lett.* **113**, 053604 (2014).
- [4] B. Pigeau, S. Rohr, L. Mercier de Lépinay, A. Gloppe, V. Jacques, and O. Arcizet, Observation of a phononic mollow triplet in a multimode hybrid spin-nanomechanical system, *Nat. Commun.* **6**, 8603 (2015).
- [5] D. A. Golter, T. Oo, M. Amezcua, K. A. Stewart, and H. Wang, Optomechanical Quantum Control of a Nitrogen-Vacancy Center in Diamond, *Phys. Rev. Lett.* **116**, 143602 (2016).
- [6] S. Hong, R. Riedinger, I. Marinkovic, A. Wallucks, S. G. Hofer, R. A. Norte, M. Aspelmeyer, and S. Gröblacher, Hanbury Brown and Twiss interferometry of single phonons from an optomechanical resonator, *Science* **358**, 203 (2017).
- [7] G. Luo, Z.-Z. Zhang, G.-W. Deng, H.-O. Li, G. Cao, M. Xiao, G.-C. Guo, L. Tian, and G.-P. Guo, Strong indirect coupling between graphene-based mechanical resonators via a phonon cavity, *Nat. Commun.* **9**, 383 (2018).
- [8] M.-A. Lemonde, S. Meesala, A. Sipahigil, M. J. A. Schuetz, M. D. Lukin, M. Loncar, and P. Rabl, Phonon Networks with Silicon-Vacancy Centers in Diamond Waveguides, *Phys. Rev. Lett.* **120**, 213603 (2018).
- [9] D. Wigger, K. Gawarecki, and P. Machnikowski, Remote phonon control of quantum dots and other artificial atoms, *Adv. Quantum Technol.* **4**, 2000128 (2021).
- [10] M. Merklein, I. V. Kabakova, T. F. S. Büttner, D.-Y. Choi, B. Luther-Davies, S. J. Madden, and B. J. Eggleton, Enhancing and inhibiting stimulated Brillouin scattering in photonic integrated circuits, *Nat. Commun.* **6**, 6396 (2015).
- [11] R. Van Laer, B. Kuyken, D. Van Thourhout, and R. Baets, Interaction between light and highly confined hypersound in a silicon photonic nanowire, *Nat. Photon.* **9**, 199 (2015).
- [12] O. Arcizet, V. Jacques, A. Siria, P. Poncharal, P. Vincent, and S. Seidelin, A single nitrogen-vacancy defect coupled to a nanomechanical oscillator, *Nat. Phys.* **7**, 879 (2011).
- [13] S. Kolkowitz, A. C. B. Jayich, Q. P. Unterreithmeier, S. D. Bennett, P. Rabl, J. G. E. Harris, and M. D. Lukin, Coherent sensing of a mechanical resonator with a single-spin qubit, *Science* **335**, 1603 (2012).
- [14] P.-B. Li, Z.-L. Xiang, P. Rabl, and F. Nori, Hybrid Quantum Device with Nitrogen-Vacancy Centers in Diamond Coupled to Carbon Nanotubes, *Phys. Rev. Lett.* **117**, 015502 (2016).
- [15] M. C. Kuzyk and H. Wang, Scaling Phononic Quantum Networks of Solid-State Spins with Closed Mechanical Subsystems, *Phys. Rev. X* **8**, 041027 (2018).
- [16] A. H. Ghadimi, S. A. Fedorov, N. J. Engelsen, M. J. Beryhi, R. Schilling, D. J. Wilson, and T. J. Kippenberg, Elastic strain engineering for ultralow mechanical dissipation, *Science* **360**, 764 (2018).
- [17] G. Calajó, M. J. A. Schuetz, H. Pichler, M. D. Lukin, P. Schneeweiss, J. Volz, and P. Rabl, Quantum acousto-optic control of light-matter interactions in nanophotonic networks, *Phys. Rev. A* **99**, 053852 (2019).
- [18] X.-L. Dong and P.-B. Li, Multiphonon interactions between nitrogen-vacancy centers and nanomechanical resonators, *Phys. Rev. A* **100**, 043825 (2019).
- [19] Q. Bin, X.-Y. Lü, F. P. Laussy, F. Nori, and Y. Wu, *n*-Phonon Bundle Emission via the Stokes Process, *Phys. Rev. Lett.* **124**, 053601 (2020).
- [20] Y.-x. Liu, A. Miranowicz, Y. B. Gao, J. Bajer, C. P. Sun, and F. Nori, Qubit-induced phonon blockade as a signature of quantum behavior in nanomechanical resonators, *Phys. Rev. A* **82**, 032101 (2010).

- [21] M. A. Kastner, Artificial atoms, *Phys. Today* **46**, 24 (1993).
- [22] W. Leonski and R. Tanas, Possibility of producing the one-photon state in a kicked cavity with a nonlinear Kerr medium, *Phys. Rev. A* **49**, R20 (1994).
- [23] A. Imamoglu, H. Schmidt, G. Woods, and M. Deutsch, Strongly Interacting Photons in a Nonlinear Cavity, *Phys. Rev. Lett.* **79**, 1467 (1997).
- [24] W. Leonski, Finite-dimensional coherent-state generation and quantum-optical nonlinear oscillator models, *Phys. Rev. A* **55**, 3874 (1997).
- [25] P. Rabl, Photon Blockade Effect in Optomechanical Systems, *Phys. Rev. Lett.* **107**, 063601 (2011).
- [26] X.-W. Xu, Y.-J. Li, and Y.-x. Liu, Photon-induced tunneling in optomechanical systems, *Phys. Rev. A* **87**, 025803 (2013).
- [27] D.-Y. Wang, C.-H. Bai, S. Liu, S. Zhang, and H.-F. Wang, Distinguishing photon blockade in a \mathcal{PT} -symmetric optomechanical system, *Phys. Rev. A* **99**, 043818 (2019).
- [28] N. Didier, S. Pugnetti, Y. M. Blanter, and R. Fazio, Detecting phonon blockade with photons, *Phys. Rev. B* **84**, 054503 (2011).
- [29] T. Ramos, V. Sudhir, K. Stannigel, P. Zoller, and T. J. Kippenberg, Nonlinear Quantum Optomechanics via Individual Intrinsic Two-Level Defects, *Phys. Rev. Lett.* **110**, 193602 (2013).
- [30] X.-W. Xu, A.-X. Chen, and Y.-x. Liu, Phonon blockade in a nanomechanical resonator resonantly coupled to a qubit, *Phys. Rev. A* **94**, 063853 (2016).
- [31] X. Wang, A. Miranowicz, H.-R. Li, and F. Nori, Method for observing robust and tunable phonon blockade in a nanomechanical resonator coupled to a charge qubit, *Phys. Rev. A* **93**, 063861 (2016).
- [32] C. Zhao, R. Peng, Z. Yang, S. Chao, C. Li, and L. Zhou, Atom-mediated phonon blockade and controlled-z gate in superconducting circuit system, *Ann. Phys.* **533**, 2100039 (2021).
- [33] R. Ohira, S. Kume, K. Takayama, S. Muralidharan, H. Takahashi, and K. Toyoda, Blockade of phonon hopping in trapped ions in the presence of multiple local phonons, *Phys. Rev. A* **103**, 012612 (2021).
- [34] H. Xie, C.-G. Liao, X. Shang, M.-Y. Ye, and X.-M. Lin, Phonon blockade in a quadratically coupled optomechanical system, *Phys. Rev. A* **96**, 013861 (2017).
- [35] L.-L. Zheng, T.-S. Yin, Q. Bin, X.-Y. Lü, and Y. Wu, Single-photon-induced phonon blockade in a hybrid spin-optomechanical system, *Phys. Rev. A* **99**, 013804 (2019).
- [36] R. Fleury, D. Sounas, M. R. Haberman, and A. Alu, Nonreciprocal acoustics, *Acoust. Today* **11**, 14 (2015).
- [37] D. L. Sounas and A. Alu, Non-reciprocal photonics based on time modulation, *Nat. Photon.* **11**, 774 (2017).
- [38] Y. Tokura and N. Nagaosa, Nonreciprocal responses from non-centrosymmetric quantum materials, *Nat. Commun.* **9**, 3740 (2018).
- [39] R. Fleury, M. R. Haberman, G. Huang, and A. N. Norris, Introduction to the special issue on non-reciprocal and topological wave phenomena in acoustics, *J. Acoust. Soc. Am.* **146**, 719 (2019).
- [40] H. Nassar, B. Yousefzadeh, R. Fleury, M. Ruzzene, A. Alu, C. Daraio, A. N. Norris, G. Huang, and M. R. Haberman, Nonreciprocity in acoustic and elastic materials, *Nat. Rev. Mater.* **5**, 667 (2020).
- [41] J. W. Strutt, Some general theorems relating to vibrations, *Proc. London. Math. Soc.* **4**, 357 (1871).
- [42] R. J. Potton, Reciprocity in optics, *Rep. Prog. Phys.* **67**, 717 (2004).
- [43] A. Metelmann and A. A. Clerk, Nonreciprocal Photon Transmission and Amplification via Reservoir Engineering, *Phys. Rev. X* **5**, 021025 (2015).
- [44] N. R. Bernier, L. D. Toth, A. Koottandavida, M. A. Ioannou, D. Malz, A. Nunnenkamp, A. K. Feofanov, and T. J. Kippenberg, Nonreciprocal reconfigurable microwave optomechanical circuit, *Nat. Commun.* **8**, 604 (2017).
- [45] A. Kamal and A. Metelmann, Minimal Models for Nonreciprocal Amplification Using Biharmonic Drives, *Phys. Rev. Appl.* **7**, 034031 (2017).
- [46] G. A. Peterson, F. Lecocq, K. Cicak, R. W. Simmonds, J. Aumentado, and J. D. Teufel, Demonstration of Efficient Nonreciprocity in a Microwave Optomechanical Circuit, *Phys. Rev. X* **7**, 031001 (2017).
- [47] X. Gu, A. F. Kockum, A. Miranowicz, Y. X. Liu, and F. Nori, Microwave photonics with superconducting quantum circuits, *Phys. Rep.* **718**, 1 (2017).
- [48] D. Malz, L. D. Toth, N. R. Bernier, A. K. Feofanov, T. J. Kippenberg, and A. Nunnenkamp, Quantum-Limited Directional Amplifiers with Optomechanics, *Phys. Rev. Lett.* **120**, 023601 (2018).
- [49] Z. Shen, Y.-L. Zhang, Y. Chen, F.-W. Sun, X.-B. Zou, G.-C. Guo, C.-L. Zou, and C.-H. Dong, Reconfigurable optomechanical circulator and directional amplifier, *Nat. Commun.* **9**, 1797 (2018).
- [50] L. M. de Lépinay, E. Damskägg, C. F. Ockeloen-Korppi, and M. A. Sillanpää, Realization of Directional Amplification in a Microwave Optomechanical Device, *Phys. Rev. Appl.* **11**, 034027 (2019).
- [51] L. M. De Lépinay, C. F. Ockeloen-Korppi, D. Malz, and M. A. Sillanpää, Nonreciprocal Transport Based on Cavity Floquet Modes in Optomechanics, *Phys. Rev. Lett.* **125**, 023603 (2020).
- [52] D.-W. Zhang, L.-L. Zheng, C. You, C.-S. Hu, Y. Wu, and X.-Y. Lü, Nonreciprocal chaos in a spinning optomechanical resonator, *Phys. Rev. A* **104**, 033522 (2021).
- [53] H. B. G. Casimir, On onsager principle of microscopic reversibility, *Rev. Mod. Phys.* **17**, 343 (1945).
- [54] J. D. Adam, L. E. Davis, G. F. Dionne, E. F. Schloemann, and S. N. Stitzer, Ferrite devices and materials, *IEEE Trans. Microw. Theory Tech.* **50**, 721 (2002).
- [55] H. Dotsch, N. Bahlmann, O. Zhuromskyy, M. Hammer, L. Wilkens, R. Gerhardt, P. Hertel, and A. F. Popkov, Applications of magneto-optical waveguides in integrated optics: Review, *J. Opt. Soc. Am. B* **22**, 240 (2005).
- [56] Y. Shi, Z. F. Yu, and S. H. Fan, Limitations of nonlinear optical isolators due to dynamic reciprocity, *Nat. Photon.* **9**, 388 (2015).
- [57] P. Aleahmad, M. Khajavikhan, D. Christodoulides, and P. LiKamWa, Integrated multi-port circulators for unidirectional optical information transport, *Sci. Rep.* **7**, 2129 (2017).

- [58] O. A. Godin, Reciprocity and energy theorems for waves in a compressible inhomogeneous moving fluid, *Wave Motion* **25**, 143 (1997).
- [59] C. Kittel, Interaction of Spin Waves and Ultrasonic Waves in Ferromagnetic Crystals, *Phys. Rev.* **110**, 836 (1958).
- [60] R. Fleury, D. L. Sounas, C. F. Sieck, M. R. Haberman, and A. Alù, Sound isolation and giant linear nonreciprocity in a compact acoustic circulator, *Science* **343**, 516 (2014).
- [61] F. Zangeneh-Nejad and R. Fleury, Doppler-based acoustic gyrator, *Appl. Sci.* **8**, 1083 (2018).
- [62] C. P. Wiederhold, D. L. Sounas, and A. Alù, Nonreciprocal acoustic propagation and leaky-wave radiation in a waveguide with flow, *J. Acoust. Soc. Am.* **146**, 802 (2019).
- [63] S. Lepri and G. Casati, Asymmetric Wave Propagation in Nonlinear Systems, *Phys. Rev. Lett.* **106**, 164101 (2011).
- [64] S. Lepri and A. Pikovsky, Nonreciprocal wave scattering on nonlinear string-coupled oscillators, *Chaos* **24**, 043119 (2014).
- [65] C. Coullais, D. Sounas, and A. Alù, Static non-reciprocity in mechanical metamaterials, *Nature* **542**, 461 (2017).
- [66] J.-G. Cui, T. Yang, and L.-Q. Chen, Frequency-preserved non-reciprocal acoustic propagation in a granular chain, *Appl. Phys. Lett.* **112**, 181904 (2018).
- [67] B. Yousefzadeh, B. Ramirez, and C. Daraio, in *APS March Meeting Abstracts*, APS Meeting Abstracts (2019), p. Y57.001.
- [68] Y. Shi, Z. Yu, and S. Fan, Limitations of nonlinear optical isolators due to dynamic reciprocity, *Nat. Photon.* **9**, 388 (2015).
- [69] S. Bhandare, S. K. Ibrahim, D. Sandel, Z. Hongbin, F. Wust, and R. Noe, Novel nonmagnetic 30-dB traveling-wave single-sideband optical isolator integrated in III/V material, *IEEE J. Sel. Top. Quantum Electron.* **11**, 417 (2005).
- [70] Z. F. Yu and S. H. Fan, Complete optical isolation created by indirect interband photonic transitions, *Nat. Photon.* **3**, 91 (2009).
- [71] H. Lira, Z. Yu, S. Fan, and M. Lipson, Electrically Driven Nonreciprocity Induced by Interband Photonic Transition on a Silicon Chip, *Phys. Rev. Lett.* **109**, 033901 (2012).
- [72] G. B. Malykin, The Sagnac effect: Correct and incorrect explanations, *Phys. Usp.* **43**, 1229 (2000).
- [73] R. Huang, A. Miranowicz, J.-Q. Liao, F. Nori, and H. Jing, Nonreciprocal Photon Blockade, *Phys. Rev. Lett.* **121**, 153601 (2018).
- [74] B. J. Li, R. Huang, X. W. Xu, A. Miranowicz, and H. Jing, Nonreciprocal unconventional photon blockade in a spinning optomechanical system, *Photonics Res.* **7**, 630 (2019).
- [75] Y.-W. Jing, H.-Q. Shi, and X.-W. Xu, Nonreciprocal Photon Blockade and Directional Amplification in a Spinning Resonator Coupled to a Two-Level Atom, *Phys. Rev. A* **104**, 033707 (2021).
- [76] N. Swindeck, S. Matsuo, K. Runge, J. O. Vasseur, P. Lucas, and P. A. Deymier, Bulk elastic waves with unidirectional backscattering-immune topological states in a time-dependent superlattice, *J. Appl. Phys.* **118**, 063103 (2015).
- [77] G. Trainiti and M. Ruzzene, Non-reciprocal elastic wave propagation in spatiotemporal periodic structures, *New J. Phys.* **18**, 083047 (2016).
- [78] Y. Wang, B. Yousefzadeh, H. Chen, H. Nassar, G. Huang, and C. Daraio, Observation of Nonreciprocal Wave Propagation in a Dynamic Phononic Lattice, *Phys. Rev. Lett.* **121**, 194301 (2018).
- [79] Y. Chen, X. Li, H. Nassar, A. N. Norris, C. Daraio, and G. Huang, Nonreciprocal Wave Propagation in a Continuum-Based Metamaterial with Space-Time Modulated Resonators, *Phys. Rev. Appl.* **11**, 064052 (2019).
- [80] J. Willis, Variational principles for dynamic problems for inhomogeneous elastic media, *Wave Motion* **3**, 1 (1981).
- [81] L. Quan, D. L. Sounas, and A. Alù, Nonreciprocal Willis Coupling in Zero-Index Moving Media, *Phys. Rev. Lett.* **123**, 064301 (2019).
- [82] Z. Yang, F. Gao, X. Shi, X. Lin, Z. Gao, Y. Chong, and B. Zhang, Topological Acoustics, *Phys. Rev. Lett.* **114**, 114301 (2015).
- [83] R. Fleury, A. B. Khanikaev, and A. Alù, Floquet topological insulators for sound, *Nat. Commun.* **7**, 11744 (2016).
- [84] A. Souslov, B. C. van Zuiden, D. Bartolo, and V. Vitelli, Topological sound in active-liquid metamaterials, *Nat. Phys.* **13**, 1091 (2017).
- [85] X. Zhou and Y. Zhao, Unusual one-way edge state in acoustic gyroscopic continuum, *Sci. China Phys. Mech. Astron.* **62**, 14612 (2018).
- [86] B. Deng, P. Wang, Q. He, V. Tournat, and K. Bertoldi, Metamaterials with amplitude gaps for elastic solitons, *Nat. Commun.* **9**, 3410 (2018).
- [87] C. Brendel, V. Peano, O. Painter, and F. Marquardt, Snowflake phononic topological insulator at the nanoscale, *Phys. Rev. B* **97**, 020102 (2018).
- [88] Y. Deng, M. Lu, and Y. Jing, A comparison study between acoustic topological states based on valley Hall and quantum spin Hall effects, *J. Acoust. Soc. Am.* **146**, 721 (2019).
- [89] Y. Ding, Y. Peng, Y. Zhu, X. Fan, J. Yang, B. Liang, X. Zhu, X. Wan, and J. Cheng, Experimental Demonstration of Acoustic Chern Insulators, *Phys. Rev. Lett.* **122**, 014302 (2019).
- [90] T. Devaux, A. Cebrecos, O. Richoux, V. Pagneux, and V. Tournat, Acoustic radiation pressure for nonreciprocal transmission and switch effects, *Nat. Commun.* **10**, 3292 (2019).
- [91] W. Fu, Z. Shen, Y. Xu, C.-L. Zou, R. Cheng, X. Han, and H. X. Tang, Phononic integrated circuitry and spin-orbit interaction of phonons, *Nat. Commun.* **10**, 2743 (2019).
- [92] B. Liang, B. Yuan, and J.-c. Cheng, Acoustic Diode: Rectification of Acoustic Energy Flux in One-Dimensional Systems, *Phys. Rev. Lett.* **103**, 104301 (2009).
- [93] A. A. Maznev, A. G. Every, and O. B. Wright, Reciprocity in reflection and transmission: What is a ‘phonon diode’?, *Wave Motion* **50**, 776 (2013).
- [94] S. Chen, C. C. Hao, C. H. Wang, Y. H. Zhang, and S. Y. Lin, One-dimensional acoustic diodes based on the anisotropy of solid media and linear acoustics, *Solid State Commun.* **206**, 38 (2015).

- [95] J.-H. He and H.-H. Huang, Multiband switching realized by a bidirectionally tunable and multiconfiguration acoustic diode, *AIP Adv.* **8**, 105032 (2018).
- [96] Y. Huang, X. Wang, X. Gong, H. Wu, D. Zhang, and D. Zhang, Contact nonlinear acoustic diode, *Sci. Rep.* **10**, 2564 (2020).
- [97] C. H. Bennett and D. P. DiVincenzo, Quantum information and computation, *Nature* **404**, 247 (2000).
- [98] D. Zueco, G. M. Reuther, S. Kohler, and P. Hänggi, Qubit-oscillator dynamics in the dispersive regime: analytical theory beyond the rotating-wave approximation, *Phys. Rev. A* **80**, 033846 (2009).
- [99] A. B. Matsko, A. A. Savchenkov, D. Strelakov, and L. Maleki, Whispering Gallery Resonators for Studying Orbital Angular Momentum of a Photon, *Phys. Rev. Lett.* **95**, 143904 (2005).
- [100] B. Y. Lao, in *1980 Ultrasonics Symposium* (1980), p. 687.
- [101] M. B. Plenio and P. L. Knight, The quantum-jump approach to dissipative dynamics in quantum optics, *Rev. Mod. Phys.* **70**, 101 (1998).
- [102] A. Miranowicz, N. Bajer, Jiříand Lambert, Y.-x. Liu, and F. Nori, Tunable multiphonon blockade in coupled nanomechanical resonators, *Phys. Rev. A* **93**, 013808 (2016).
- [103] A. Miranowicz, M. Paprzycka, Y.-x. Liu, J. Bajer, and F. Nori, Two-Photon and Three-Photon Blockades in Driven Nonlinear Systems, *Phys. Rev. A* **87**, 023809 (2013).
- [104] C. Hamsen, K. N. Tolazzi, T. Wilk, and G. Rempe, Two-Photon Blockade in an Atom-Driven Cavity QED System, *Phys. Rev. Lett.* **118**, 133604 (2017).
- [105] M. E. Levinstein, S. L. Rumyantsev, and M. S. Shur, *Properties of Advanced Semiconductor Materials: GaN, AlN, InN, BN, SiC, SiGe* (John Wiley & Sons, New York, 2001).
- [106] T. Azuhata, M. Takesada, T. Yagi, A. Shikanai, S. Chichibu, K. Torii, A. Nakamura, T. Sota, G. Cantwell, D. B. Eason, and C. W. Litton, Brillouin scattering study of ZnO, *J. Appl. Phys.* **94**, 968 (2003).
- [107] B. A. Auld, *Acoustic Fields and Waves in Solids* (Wiley, New York, 1973).
- [108] R. O. Pohl, X. Liu, and E. Thompson, Low-temperature thermal conductivity and acoustic attenuation in amorphous solids, *Rev. Mod. Phys.* **74**, 991 (2002).
- [109] C. M. Flannery, M. D. Whitfield, and R. B. Jackman, Acoustic wave properties of CVD diamond, *Semicond. Sci. Technol.* **18**, S86 (2003).
- [110] S. Datta, *Surface Acoustic Wave Devices* (Prentice-Hall, Upper Saddle River, NJ, 1986).
- [111] D. Morgan, *Surface Acoustic Wave Filters* (Academic Press, Boston, 2007).
- [112] W. Wang, M. Shen, C.-L. Zou, W. Fu, Z. Shen, and H. X. Tang, High-acoustic-index-contrast phononic circuits: Numerical modeling, *J. Appl. Phys.* **128**, 184503 (2020).
- [113] P. Rabl, P. Cappellaro, M. V. G. Dutt, L. Jiang, J. R. Maze, and M. D. Lukin, Strong magnetic coupling between an electronic spin qubit and a mechanical resonator, *Phys. Rev. B* **79**, 041302 (2009).
- [114] K. D. Petersson, J. R. Petta, H. Lu, and A. C. Gossard, Quantum Coherence in a One-Electron Semiconductor Charge Qubit, *Phys. Rev. Lett.* **105**, 246804 (2010).
- [115] M. Metcalfe, S. M. Carr, A. Muller, G. S. Solomon, and J. Lawall, Resolved Sideband Emission of InAs/GaAs Quantum Dots Strained by Surface Acoustic Waves, *Phys. Rev. Lett.* **105**, 037401 (2010).
- [116] K. V. Kepesidis, S. D. Bennett, S. Portolan, M. D. Lukin, and P. Rabl, Phonon cooling and lasing with nitrogen-vacancy centers in diamond, *Phys. Rev. B* **88**, 064105 (2013).
- [117] I. Yeo, P. L. de Assis, A. Gloppe, E. Dupont-Ferrier, P. Verlot, N. S. Malik, E. Dupuy, J. Claudon, J. M. Gérard, A. Auffèves, G. Nogues, S. Seidelin, J. P. Poizat, O. Arcizet, and M. Richard, Strain-mediated coupling in a quantum dot–mechanical oscillator hybrid system, *Nat. Nanotechnol.* **9**, 106 (2014).
- [118] S. J. Whiteley, G. Wolfowicz, C. P. Anderson, A. Bourassa, H. Ma, M. Ye, G. Koolstra, K. J. Satzinger, M. V. Holt, F. J. Heremans, A. N. Cleland, D. I. Schuster, G. Galli, and D. D. Awschalom, Spin-phonon interactions in silicon carbide addressed by Gaussian acoustics, *Nat. Phys.* **15**, 490 (2019).
- [119] J. V. Cady, O. Michel, K. W. Lee, R. N. Patel, C. J. Sarabalis, A. H. Safavi-Naeini, and A. C. B. Jayich, Diamond optomechanical crystals with embedded nitrogen-vacancy centers, *Quantum Sci. Technol.* **4**, 024009 (2019).
- [120] B. Li, P.-B. Li, Y. Zhou, J. Liu, H.-R. Li, and F.-L. Li, Interfacing a Topological Qubit with a Spin Qubit in a Hybrid Quantum System, *Phys. Rev. Appl.* **11**, 044026 (2019).
- [121] A. Vogeles, M. M. Sonner, B. Mayer, X. Yuan, M. Weiß, E. D. S. Nysten, S. F. Covre da Silva, A. Rastelli, and H. J. Krenner, Quantum dot optomechanics in suspended nanophononic strings, *Adv. Quantum Technol.* **3**, 1900102 (2020).
- [122] E. D. S. Nysten, A. Rastelli, and H. J. Krenner, A hybrid (Al)GaAs-LiNbO₃ surface acoustic wave resonator for cavity quantum dot optomechanics, *Appl. Phys. Lett.* **117**, 121106 (2020).
- [123] X.-L. Dong, P.-B. Li, T. Liu, and F. Nori, Unconventional Quantum Sound-Matter Interactions in Spin-Optomechanical-Crystal Hybrid Systems, *Phys. Rev. Lett.* **126**, 203601 (2021).
- [124] M. Weiß, D. Wigger, M. Nägele, K. Müller, J. J. Finley, T. Kuhn, P. Machnikowski, and H. J. Krenner, Optomechanical wave mixing by a single quantum dot, *Optica* **8**, 291 (2021).
- [125] X.-X. Li, P.-B. Li, H.-R. Li, H. Gao, and F.-L. Li, Simulation of topological zak phase in spin-phononic crystal networks, *Phys. Rev. Res.* **3**, 013025 (2021).
- [126] H. Okamoto, A. Gourgout, C.-Y. Chang, K. Onomitsu, I. Mahboob, E. Y. Chang, and H. Yamaguchi, Coherent phonon manipulation in coupled mechanical resonators, *Nat. Phys.* **9**, 480 (2013).
- [127] M. J. A. Schuetz, E. M. Kessler, G. Giedke, L. M. K. Vandersypen, M. D. Lukin, and J. I. Cirac, Universal Quantum Transducers Based on Surface Acoustic Waves, *Phys. Rev. X* **5**, 031031 (2015).

- [128] M. W. Doherty, N. B. Manson, P. Delaney, F. Jelezko, J. Wrachtrup, and L. C. L. Hollenberg, The nitrogen-vacancy colour centre in diamond, *Phys. Rep.* **528**, 1 (2013).
- [129] P.-B. Li and F. Nori, Hybrid Quantum System with Nitrogen-Vacancy Centers in Diamond Coupled to Surface-Phonon Polaritons in Piezomagnetic Superlattices, *Phys. Rev. Appl.* **10**, 024011 (2018).
- [130] C. Bradac, W. Gao, J. Forneris, M. E. Trusheim, and I. Aharonovich, Quantum nanophotonics with group IV defects in diamond, *Nat. Commun.* **10**, 5625 (2019).
- [131] P.-B. Li, Y. Zhou, W.-B. Gao, and F. Nori, Enhancing Spin-Phonon and Spin-Spin Interactions Using Linear Resources in a Hybrid Quantum System, *Phys. Rev. Lett.* **125**, 153602 (2020).
- [132] P. Chalker, T. Joyce, C. Johnston, J. Crossley, J. Huddleston, M. Whitfield, and R. Jackman, Fabrication of aluminium nitride/diamond and gallium nitride/diamond saw devices, *Diamond Relat. Mater.* **8**, 309 (1999).
- [133] H. Nakahata, S. Fujii, K. Higaki, A. Hachigo, H. Kitabayashi, S. Shikata, and N. Fujimori, Diamond-based surface acoustic wave devices, *Semicond. Sci. Technol.* **18**, S96 (2003).
- [134] H. Ishiwata, M. Nakajima, K. Tahara, H. Ozawa, T. Iwasaki, and M. Hatano, Perfectly aligned shallow ensemble nitrogen-vacancy centers in (111) diamond, *Appl. Phys. Lett.* **111**, 043103 (2017).
- [135] L.-x. Chen, H. Liu, S. Liu, C.-m. Li, Y.-c. Wang, K. An, C.-y. Hua, J.-l. Liu, J.-j. Wei, L.-f. Hei, and F.-x. Lv, Growth of high quality AlN films on CVD diamond by rf reactive magnetron sputtering, *Appl. Surf. Sci.* **431**, 152 (2018).
- [136] J. Lang, S. Häußler, J. Fuhrmann, R. Waltrich, S. Laddha, J. Scharpf, A. Kubanek, B. Naydenov, and F. Jelezko, Long optical coherence times of shallow-implanted, negatively charged silicon vacancy centers in diamond, *Appl. Phys. Lett.* **116**, 064001 (2020).
- [137] D. A. Golter, T. Oo, M. Amezcua, I. Lekavicius, K. A. Stewart, and H. Wang, Coupling a Surface Acoustic Wave to an Electron Spin in Diamond via a Dark State, *Phys. Rev. X* **6**, 041060 (2016).
- [138] M. V. Gustafsson, T. Aref, A. F. Kockum, M. K. Ekström, G. Johansson, and P. Delsing, Propagating phonons coupled to an artificial atom, *Science* **346**, 207 (2014).
- [139] R. Manenti, A. F. Kockum, A. Patterson, T. Behrle, J. Rahamim, G. Tancredi, F. Nori, and P. J. Leek, Circuit quantum acoustodynamics with surface acoustic waves, *Nat. Commun.* **8**, 975 (2017).
- [140] B. A. Moores, L. R. Sletten, J. J. Viennot, and K. W. Lehnert, Cavity Quantum Acoustic Device in the Multimode Strong Coupling Regime, *Phys. Rev. Lett.* **120**, 227701 (2018).
- [141] K. J. Satzinger, Y. P. Zhong, H. S. Chang, G. A. Peairs, A. Bienfait, M.-H. Chou, A. Y. Cleland, C. R. Conner, E. Dumur, J. Grebel, I. Gutierrez, B. H. November, R. G. Povey, S. J. Whiteley, D. D. Awschalom, D. I. Schuster, and A. N. Cleland, Quantum control of surface acoustic-wave phonons, *Nature* **563**, 661 (2018).